Author Manuscript

Instantaneous radiative effect of surface longwave spectral emissivity in a Snowball Earth simulation

Daniel S. Zetterberg[1], Xianglei Huang[1], Johannes Hörner[2], Aiko Voigt[2], and Xiuhong Chen[1]

[1]Department of Climate and Space Sciences and Engineering, the University of Michigan, Ann Arbor, MI, USA.
[2]Department of Meterology and Geophysics, University of Vienna, Vienna, Austria.

Corresponding author: Xianglei Huang (xianglei@umich.edu)

Key Points:

- Surface spectral emissivity has a moderate impact on the top-of-atmosphere radiation budget in the cold and dry Snowball Earth climate.
- Compared to the assumed blackbody, realistic surface emissivity can reduce global-mean outgoing longwave radiation by 1.0-2.9 W m^{-2}.
- The effect is greater for ice than snow, highlighting the impact of precipitation processes on radiation budgets in Snowball Modeling.

This is the author manuscript accepted for publication and has undergone full peer review but has not been through the copyediting, typesetting, pagination and proofreading process, which may lead to differences between this version and the Version of Record. Please cite this article as doi: 10.1029/2025JD043596.

This article is protected by copyright. All rights reserved.

Author Manuscript

Abstract

Spectrally dependent emission by the surface (i.e., surface spectral emissivity) is commonly ignored by current climate models. Surface spectral emissivity matters more in cold and dry environments than in hot and humid environments. Recent modeling studies confirmed that, for current climate simulations, this process affects the polar climate more than the extra-polar climate. As for the Snowball Earth, a period characterized by global polar-like conditions of extreme cold and low humidity, including surface spectral emissivity could alter the simulated global radiation budget. This, in turn, could affect the simulated climate of the Snowball Earth. Here, we use an aqua-planet slab-ocean simulation of Snowball Earth by the ICON model to perform offline radiative transfer calculations to quantify such impact on the outgoing longwave radiation (OLR). The offline radiative transfer model is used to compute the clear-sky OLR for two surfaces that would be present in the extremely cold simulation: ice and snow. Compared to the results with assumed blackbody surface, the global mean OLR decreases by 2.9 and 1.0 W m^{-2} for ice and snow surfaces, respectively. The impact of surface spectral emissivity on the OLR is strongest at the equator and weakens towards the poles, presenting a noticeable meridional gradient. Effects of surface emissivity are also larger during the summer than the winter. The radiative effects of this often-neglected process would be small for a snow-covered globe but could be important for climate states with exposed ice, particularly Jormungand states, as well as simulations of other cold and dry climates.

Plain Language Summary

Approximately 600 million years ago, Earth was covered in sea ice and glaciers in an extreme climate state known as the Snowball Earth. Surface spectral emissivity is a radiative process that is ignored in most climate models but could have a strong effect on Snowball simulations. Surface spectral emissivity means that the efficiency with which a surface emits radiation depends on the radiation's wavelength. When surface spectral emissivity is included in models of the current climate, the radiation that escapes from the Earth system is reduced, particularly at the poles where low humidity renders the radiation budget sensitive to these processes. To quantify the effect of this process on the Snowball Earth, which has global polar-like conditions, the radiation budget was calculated for typical Snowball conditions, with this process included. We found that, for a snow-covered Snowball Earth, surface spectral emissivity would decrease the radiation that the Earth system emits by 0.9%. Compared to other uncertainties in modeling this climate state, this is a negligible difference. However, for glaciation scenarios with exposed ice, surface emissivity could be important, as the global reduction in outgoing longwave radiation for an ice surface is 2.9%.

1 Introduction

According to the Snowball Earth Hypothesis, ice and glaciers extended down to the tropics during several periods between 1,000 and 500 million years ago (Ma), forming one of the most extreme climate states in Earth's history (Kirschvink, 1992; Hoffman et al., 1998). Climate models have been extensively used to understand the climate in this era (e.g., Pierrehumbert et al., 2011; Liu et al., 2010; Voigt et al., 2011; Yang et al., 2012; Abbot et al., 2013). Because of the scant evidence from when these Snowball events occurred and the

This article is protected by copyright. All rights reserved.

extreme conditions divergent from those of the present climate, we might not have a full understanding of all physical processes important for the Snowball Earth climate. Certain physical processes that have been ignored in models designed to simulate the current climate might play non-negligible roles in the modeling of the Snowball Earth. Additionally, for some physical processes and properties that have been included in models of the current climate, more detailed representations may need to be considered for the Snowball Earth simulation. For example, sea ice grew thicker and at latitudes that it does not reach in the present climate (Hoffman & Schrag, 2002). As a result, more physical processes that deal with the dynamics, thermodynamics, and radiative transfer of ice and snow might need to be incorporated into models to more accurately delineate the impact of low-latitude ice on the climate (e. g. Abbot et al., 2010; Voigt & Abbot, 2012; Hörner et al., 2022; Hörner & Voigt, 2024).

It is well known that ice-albedo feedback exerts a strong influence on the Snowball Earth climate (Hoffman et al., 2017). The key radiative process is the difference in albedo between ice and ocean. As the Earth cools and surface temperatures decrease, oceans freeze and the average latitudinal ice line moves towards the Equator. The ice and snow of the frozen oceans have much higher albedos than the liquid oceans, so more sunlight is reflected back to space, leaving the energy balance of the Earth system in the negative. To compensate for this imbalance, the global surface temperature decreases, and even more oceans freeze, which forms a positive feedback normally referred to as ice-albedo feedback. The early Budyko-Sellers climate model (Budyko 1969, Sellers 1969) elegantly showed an unstable regime in which this positive feedback can result in a completely ice-covered world. Subsequent more complicated three-dimensional climate model simulations further corroborate the importance of this shortwave surface albedo feedback, as described in the section “Sea-glacier development on the Snowball ocean” of Hoffman et al. (2017) and the references therein. Pierrehumbert (2010) explored the impact of the spectral albedo of ice. They found that using a more realistic two-band model for ice albedo, with a higher albedo in the visible portion of the spectrum than the near-infrared portion of the spectrum, resulted in little change to the Snowball Earth climate, as the majority of ice in their simulation was covered by snow.

Different surfaces can have not only different albedos in the shortwave, but also different emissivities in the longwave. Moreover, like albedo, such emissivity can vary with wavelength. While the atmospheric radiation schemes in the climate models usually take surface spectral albedo into account to some extent, they typically assume all surfaces to be blackbody (i.e., a unity emissivity through the entire longwave) or a graybody with emissivity of nearly one (e.g. 0.996 in the ECHAM model, Stevens & Schwartz, 2012) for computational efficiency. In reality, surface emissivity can deviate from unity and significantly vary with frequency, as shown in Figure 1. Surface types expected in a Snowball Earth, such as ice, snow, and ocean, exhibit different spectral dependences in their emissivities, especially for 0 – 1000 cm^{-1} (>10 μm in wavelength). According to Wien’s displacement law, the colder the surface is, the more emission is dominated by longer wavelengths of the spectrum. For example, for a 288 K (roughly the global mean surface temperature of the current climate) blackbody, 28.9% of its radiation comes from 0-500 $cm^{-1,}$ and 75.4% comes from 0-1000 cm^{-1}. But for a 200 K blackbody, the contributions from 0-500 cm^{-1} and 0-1000 cm^{-1} become 51.9% and 93.3%, respectively. The large differences in surface emissivities among ocean, ice, and snow occur in

This article is protected by copyright. All rights reserved.

Author Manuscript

the spectral region that dominates the surface longwave emission of the Snowball Earth. Therefore, it is worth investigating by how much the blackbody assumption adopted by climate models can cause an incorrect representation of longwave radiation processes when such models are used in Snowball Earth simulations.

Recent studies have quantified the influence of surface spectral emissivity on simulations of the current climate. Using offline radiative transfer calculations, Chen et al. (2014) pointed out that the impact of surface spectral emissivity on the top-of-atmosphere (TOA) radiance budget is non-negligible. When realistic surface spectral emissivity was incorporated into a global climate model (GCM), the mean-state surface temperature in polar regions differed by as much as +1 K (Huang et al., 2018). Correspondingly, the sea ice fraction was shown to have a statistically significant reduction (Huang et al., 2018). Feldman et al. (2014) found that incorporating surface spectral emissivity could enhance modelled global warming in the Arctic. Manzo et al. (2025) explored various methods of formulating graybody and spectral band-averaged surface emissivities and showed that using a five-spectral-band model can significantly reduce biases in longwave radiative heating rate calculations. The impact of surface spectral emissivity on the simulated regional climate of the Sahara and Sahel areas has also been studied (Chen et al., 2019). The implications of Chen et al. (2014) and Huang et al. (2018) for Snowball Earth simulation can be summarized as follows. On most of the Earth's surface in the present day, water vapor renders the atmosphere opaque in the far-infrared (IR) portion of the spectrum. However, due to the low temperature and low specific humidity of polar regions, the total column water vapor (TCWV) is greatly reduced compared to the rest of the globe. With weaker atmospheric far-IR absorption, more surface far-IR radiation can reach space, so surface emissivity has a greater effect on the polar energy budget than it does on the rest of the globe. Note that virtually everywhere on the Snowball Earth has a colder and drier atmosphere than the polar regions of the current Earth. Therefore, including a surface emissivity that is accurate across the longwave spectrum could affect the simulated Snowball Earth climate in a noticeable way.

This study seeks to quantify the TOA instantaneous radiative effect of including surface emissivity on a Snowball Earth-like climate. Two surface types are comprehensively examined in this study, namely, ice and snow; for comparison purpose, single-column results for the ocean surface are also examined. The rest of this paper is organized as follows: Section 2 describes the simulation data and radiative transfer model used in the study; Section 3 presents the instantaneous radiative effect of including surface spectral emissivity; and Section 4 discusses how such radiative effects could contribute to open questions in Snowball Earth modeling and paleoclimate modeling in general.

2 Methodology

2.1 Simulation data

In this study, we use a Snowball Earth simulation from Hörner & Voigt (2024) that resulted in sea ice covering the entire aqua planet, representative of the formation of a hard Snowball state. The ICOsahedral Non-hydrostatic Atmospheric model, ICON-A, was used in the simulation. Details regarding the ICON-A model can be found in Giorgetta et al. (2018). The

This article is protected by copyright. All rights reserved.

Author Manuscript

ICON-A model was coupled to a 50-meter slab-ocean model for an aqua planet configuration. 1285 W m^{-2} was used as an estimate of the Neoproterozoic solar constant. CO_2 concentration was set to 5000 ppmv, well mixed throughout the atmosphere. Besides CO_2, water vapor, and ozone, the rest of the greenhouse gases were set to zero, for simplicity, in the simulations depicted in Hörner & Voigt (2024). Hörner and Voigt (2024) analyzed the impact of different choices of ice thermodynamics schemes on the ice line of a Snowball Earth model. The results used here were from the simulation using the control Semtner scheme for the ice thermodynamics. Further details of the simulation, as well as the ice thermodynamic schemes, can be found in Hörner & Voigt (2024) and Hörner et al. (2022).

The climatological zonal-mean surface and atmospheric temperatures of the simulation are shown in Figure 2. The temperature of the modeled Snowball Earth is significantly colder than the present Earth. Notably, there is no strong contrast between surface and atmospheric temperature outside the Tropics (30°S to 30°N). The near-surface temperature inversion is ubiquitous in the extra-tropical regions (also shown in Figure 3b). For the mid-latitude and polar regions, the lapse rates from the near-surface temperature inversion to the tropopause are about 2.1 and 3.1 K/km, respectively. The tropical lapse rate, 7.2 K/km, is closer to that of the current Earth. The climatological zonal-mean TCWV of the simulation is shown in Figure 3. For comparison, the zonal-mean TCWV in the current climate, i.e., the 10-year average (2006-2015) based on the NASA-MERRA 2 reanalysis (Gelaro et al., 2017), is shown in Table 1. There is a 2-3 orders of magnitude difference in the TCWV between the current climate and the simulated Snowball Earth.

2.2 Radiative transfer model

The radiative transfer model used in this study is the MODerate resolution atmospheric TRANsmission code (MODTRAN) version 5.2.0 developed by Spectral Science Inc and previously Air Force Research Laboratory (Berk et al., 2005). It is a radiative transfer model extensively used by the atmospheric radiation community. It can correctly handle a wide range of temperature and greenhouse gas profiles, including those in the Snowball Earth regime. It can calculate the spectral flux at a resolution of 0.1 cm^{-1} with satisfactory performance compared to the benchmark line-by-line radiative transfer model, with a difference of only up to a few percent (Anderson et al., 2006). More details of this code can be found in Berk et al. (1998), Berk et al. (2005) and Anderson et al. (2006).

2.3 Calculation procedure

We use MODTRAN to calculate the effect of surface spectral emissivity on the outgoing longwave radiation (OLR) using the modeled atmospheric profiles from the aforementioned Snowball Earth simulation as the inputs. Here OLR is defined as positive, so a reduction in OLR would have a warming effect. The ICON-A simulation output was interpolated from the native icosahedral grid onto a $4^{\circ}\times5^{\circ}$ regular grid. The same greenhouse gas configurations as used by the original Snowball Earth simulation are used in MODTRAN calculations. Calculations were performed using the same atmospheric profiles but different surface types, namely blackbody, ice, snow, and ocean surfaces (with ocean used only for comparison purpose). The specific

This article is protected by copyright. All rights reserved.

Author Manuscript

spectral emissivities come from a global surface spectral emissivity dataset compiled by Huang et al. (2016a). For each calculation, the surface of the entire globe was replaced by the surface type in question. For example, for the ice calculation, the surface emissivity of each grid cell was changed to that of ice. The deviation from the results using a blackbody surface is deemed as the instantaneous radiative effect of the specific surface. The result is the OLR change when ice or snow spectral emissivities are used for every point on the globe. Calculations were done for the clear-sky only, i.e., the maximum instantaneous radiative effect that surface spectral emissivity can cause. Given the popularity of the RRTMG LW radiation scheme (Iacano et al., 2008; Mlawer et al., 1997) in the climate modeling community, the impact on the band-integrated flux over individual RRTMG LW bands will be discussed. Due to the small longitudinal contrast in the simulation, discussions below will focus on the zonal-mean effects.

In addition to the comprehensive analysis of the effects of the ice and snow surface types, calculations were also performed using an ocean surface type. Note that the atmosphere used comes from an ice-covered simulation. As such, the atmospheric conditions are colder and drier than those from a climate state with an open ocean. Therefore, using the ocean surface emissivity does not present a physical estimate of how OLR would change in a Snowball simulation if ocean surface emissivity were used. Nevertheless, the results using the ocean surface are still included for completeness, and they represent an upper bound on the effect of ocean emissivity. The ocean results can also be thought of as the effect on single-column OLR for small-scale ocean features that could appear in the hard Snowball Earth, such as leads and sea ice fractures.

3 Results

3.1 A graybody sensitivity study

Before using realistic, spectrally dependent surface emissivity in the calculation, we first investigate the sensitivity of OLR to graybody emissivity with varying TCWV in representative Snowball Earth scenarios. This is one step away from the blackbody or near-blackbody assumption used in many current models. Starting from Schwarzschild's Law (Schwarzschild 1914) and following Huang et al. (2018), the sensitivity of the spectral OLR (denoted by F_{TOA}) at a given frequency can be written as:

$$\frac{\partial F_{TOA}}{\partial \epsilon} = \left(\pi B\left(T_{surf}\right) - F_{atm}^{\downarrow}\right) e^{-\tau^*} \quad (1)$$

where ϵ is the surface emissivity, $B\left(T_{surf}\right)$ is the blackbody emission of the surface, $F_{atm}^{\downarrow}$ is the atmospheric downward longwave radiation at the surface, and τ^* is the diffusive atmospheric optical depth. Every term here is spectrally dependent, so the subscript denoting frequency is omitted for brevity. If the atmosphere is opaque at a given frequency (i.e., $\tau^* \to +\infty$) the outgoing radiation has little sensitivity on the surface emissivity because $e^{-\tau^*}$ approaches zero. In a translucent atmosphere, the sign of $\frac{\partial F_{TOA}}{\partial \epsilon}$ would depend on the contrast between the

This article is protected by copyright. All rights reserved.

surface emission and the downward flux at the surface. The sensitivity would be positive as long as the surface emission is higher than the downward flux at the surface.

For three typical climate zones, i.e., tropics (30 S – 30 N), mid-latitude (30 – 60 S and 30 - 60 N), and polar regions (60 – 90 S and 60 – 90 N), we obtained averaged temperature and humidity profiles from the ICON simulation, shown in Figure 3b. The humidity profiles were scaled such that the TCWV varies from 0 to 10 mm to study the sensitivity of OLR to emissivity for a wide range of humidity, from Snowball Earth levels to the present level. The surface was assumed to be a graybody, and MODTRAN was used to numerically calculate $\frac{\partial F_{TOA}}{\partial \epsilon}$ for different TCWV by calculating F_{TOA} while surface emissivity was varied. The results are summarized in Figure 4. For a 1% change in surface emissivity, the change in OLR can be ~0.5 W m^{-2} for the polar region and ~1.1 W m^{-2} for the tropics. Consistent with what Eq (1) suggests, Figure 4a shows that the sensitivity decreases as TCWV increases because an increase of TCWV leads to an increase of downward flux at the surface and a decrease in atmospheric transmissivity. This result is consistent with the results of Chen et al. (2014) (see its Figure 1) and Manzo et al. (2025) (see its Figure 7c). For all TCWV, the warmer the region is, the larger the $\frac{\partial F_{TOA}}{\partial \epsilon}$ is simply because the warmer surface results in more upward emission. However, when looking at the effect of surface emissivity on F_{TOA} relative to the blackbody value of $F_{TOA,}$ i.e. (dF/F)/dϵ vs TCWV, in Figure 4b, the curves for different regions are closer together. For a TCWV value near 0, as in the case of the actual Snowball Earth simulation, a 1% change in surface emissivity would decrease F_{TOA} by 0.75 - 0.80%. Given that the emissivities for snow, ice, and ocean surfaces differ from unity by more than 1%, the modeled OLR of the Snowball Earth is susceptible to including this process. However, considering the global conditions of the modeled Snowball Earth, the low values of TCWV combined with the prevalence of strong temperature inversions at even mid-latitudes complicate the understanding of the impact of including surface spectral emissivity. Therefore, detailed radiative transfer calculations must be made to quantify the impact of including this feature in models.

3.2 Longwave broadband effects

Figure 5 shows the absolute and relative differences of zonal-mean OLR when the spectral emissivities of ice and snow surfaces are used instead of a blackbody surface in the MODTRAN offline radiative transfer calculations. In addition, Figure 5 depicts calculations performed for an ocean surface (blue dashed line). Note that the results for the ocean surface do not represent the zonal-mean OLR change, as any large open ocean would come from a warmer and more humid environment. Instead, the ocean case results represent the instantaneous OLR change from surface spectral emissivity for a single column, such as for a small lead opening up in the sea ice. Such results are presented as a function of latitude.

When the surface spectral emissivity of ice is used, the difference is around 3 W m^{-2} in the tropics, around 3% of the OLR. Towards the poles, the absolute difference decreases to around 2 W m^{-2}, but the relative differences increase to up to 3.8%. When the snow surface emissivity is used, the difference is much smaller, with the relative difference being near 1% at all latitudes. When the ocean emissivity is used, the differences are even larger than those from

This article is protected by copyright. All rights reserved.

Author Manuscript

the ice surface case, though this represents an upper bound on the ocean case, as noted earlier. Such results are consistent with what has been shown in Figure 1: ice emissivity has larger deviations from unity than snow emissivity does, especially in the far-IR. Therefore, the OLR difference caused by an ice surface is larger than the counterpart by a snow surface. Globally averaged OLR reductions from the blackbody calculation are 2.9 W m^{-2} for ice surface and 1.0 W m^{-2} for snow surface, respectively.

Following Eq (1), the impact of surface spectral emissivity is determined by the balance between the surface emission to space and reflection of downward atmospheric emission. For the ice surface case, surface reflection of atmospheric emission can contribute around 1 W m^{-2} to OLR, which reduces the effect of surface emissivity on OLR. However, due to the surface emission being greater than the downward flux at the surface, any reduction from unity for the surface emissivity will cause a net reduction in OLR for Snowball Earth climate simulations.

3.3 Band-by-band radiative effects

Here we further examine the impact of different surface spectral emissivities on TOA flux over individual bands. Our spectral calculation is done at 2 cm^{-1} resolution (full-width-half-maximum) and then integrated over the RRTMG bandwidths, which are shown in Figure 6. Table 2 lists the bandwidth of each band, as well as the significant absorbers in each band. These features are also depicted in Figure 6c, which shows a mid-latitude emission spectrum from our blackbody calculations and the RRTMG wavenumber boundaries. In this spectrum, note that the far-IR emission appears relatively smooth because the wavenumber resolution of our calculations averages out the far-IR water vapor absorption lines. We omit discussion of RRTMG longwave bands 13-16 (corresponding to wavenumbers of 2080-3250 cm^{-1}) because the emission spectrum of the cold Snowball Earth climate is shifted to lower wavenumbers, resulting in these bands contributing little to OLR (i.e. less than 0.015%). For the Snowball climate, the far-IR bands (i.e. RRTMG bands 1-3) are the most prominent contributors to OLR, rather than the atmospheric window bands, as is the case for the current climate. Several noteworthy features in Figure 6 are discussed below:

(1) There is no flux difference in RRTMG Band 4 (630-700 cm^{-1}) because this band features strong CO_2 absorptions and emissions in the atmosphere. The atmosphere is so opaque in this band that surface emission cannot reach the TOA at all, making the TOA flux insensitive to the choice of surface emissivity. This is seen in the Band 4 spike in the emission spectrum of Figure 6c.

(2) Consistent with the spectral emissivities shown in Figure 1, the results of the snow surface have small deviations from that of a blackbody surface, with no more than 2.5% difference in any band.

(3) Ice surface has moderate differences, up to 5.1%, in the far-IR bands, especially the 2nd band from 350 to 500 cm^{-1}. As labeled in Figure 6, the three far-IR bands account for around 65% of the globally-averaged clear-sky OLR for the case of blackbody surfaces. Such a large

This article is protected by copyright. All rights reserved.

Author Manuscript

fractional change also implies a large absolute flux change due to the surface emissivities in the far-IR.

Besides Band 4, the relative differences in different bands exhibit two forms of meridional gradients caused by absorption and emission features from different greenhouse gases. In bands dominated by water vapor absorptions and emissions, such as Bands 1, 2, 10, and 11, the magnitude of the relative difference increases from the tropics to both poles. As shown in Figure 3(a), the TCWV of the Snowball simulation is greater in the tropics than in the polar regions. Therefore, as latitude increases, the amount of water vapor absorption decreases, and the atmosphere becomes optically thinner. This allows more surface radiation in these bands to reach the TOA, making the TOA flux in these bands more sensitive to changes in surface emissivity. Band 5 displays the opposite meridional gradient: the relative difference decreases as the absolute value of latitude increases. Band 5 contains CO_2 absorption and emission features, but unlike Band 4, it is not opaque, so the surface emission can still reach the TOA. Note that CO_2 is well mixed throughout the atmosphere, so the meridional gradient of its optical depth should be much smaller than that of H_2O. The atmospheric temperature meridional gradient is weaker than that of surface temperature, as displayed in Figure 2. Because the atmospheric effective emission depends on temperature and optical depth, the change of such atmospheric effective emission in Band 5 from the equator to the poles is much less than the decrease in surface emission from the equator to the poles. Since only surface emission is impacted by including surface emissivity, the relative difference of surface emissivity on the band OLR is thus weaker in the polar regions than the equator. Band 7, which features ozone absorption and emission, also displays a weaker version of this meridional pattern.

3.4 Seasonal cycle

Due to the lack of exposed ocean, models have shown that the seasonal temperature cycle of the Snowball Earth can be large, with temperature swings as great as 50 K per year (Liu et al., 2020). Such seasonal variation in the conditions of the Snowball Earth leads us to further investigate the seasonal variations of the effect of surface spectral emissivity on OLR using the monthly output of the same Snowball simulation. Figure 7 summarizes such seasonal differences.

Due to the circular orbit and homogenous surface used in the aqua-planet simulation, the seasonal cycle is only determined by the Earth's obliquity, resulting in symmetric seasonal variations in two hemispheres: the seasonal-mean climatology of both hemispheres is essentially the same. The seasonal cycle of the effect of surface emissivity on OLR is thus symmetric across the two hemispheres. When realistic surface spectral emissivity is included, the summertime OLR reduction is greater than the annual-mean OLR reduction, which can be as much as 3.7 W m^{-2} for an ice surface. Wintertime OLR reduction is less but remains significant for the case of an ice surface. For summer and winter, the deviation from the annually averaged radiative effect is higher in the polar regions than in the tropics. Such seasonal variation of OLR reduction due to the inclusion of realistic surface emissivity is decided

This article is protected by copyright. All rights reserved.

Author Manuscript

mainly by the seasonal variation of surface longwave emission, instead of the seasonal variation of reflection of downward longwave flux at the surface. The higher the surface temperature is, the greater the reduction in surface infrared emission caused by a non-blackbody surface. This is the primary reason why the magnitude of such OLR reduction is larger in the summer than in the winter for all latitudes. This also explains why the seasonal variation of such an effect in OLR is larger in the polar region than in the tropics, as the surface temperature in the polar region experiences a much larger seasonal cycle than its counterpart in the tropics.

4 Conclusions and discussions

Using realistic surface spectral emissivity instead of a simple blackbody assumption with the atmospheric profiles derived in a hard Snowball Earth simulation can lead to a globally averaged OLR reduction of 2.9 W m^{-2} for ice surface and 1.0 W m^{-2} for snow surface. Such an effect on the OLR is larger in the tropics than in the polar regions. The effect is more pronounced for the ice surface than for the snow surface because the former has a larger deviation from blackbody in the far-IR. Thus, the effect strongly depends on snow cover. A reduction in the OLR implies that, when such surface spectral emissivity treatment is included in the climate model simulations, it would reduce the OLR and warm the simulated surface climate. Then the radiative feedbacks would respond to such changes and eventually affect the simulated climate mean state.

Using the surface cover from the ICON simulation and a simple forcing-feedback framework, the global change in surface air temperature when surface emissivity is included in a Snowball Earth model can be estimated. In the ICON simulation, the minimum zonal-average snow thickness was 20 cm, though at a few grid cells in the tropics the snow thickness was less than one cm. Effectively, the simulated Snowball formation resulted in a snow-covered world. With only Planck feedback, a rough estimate of temperature change ($\boldsymbol{\Delta T}$) due to forcing is:

$$\boldsymbol{\Delta T \approx \Delta F \left(\frac{\partial F}{\partial T}\right)^{-1} = \frac{\Delta F}{4\sigma T^3}} \qquad (2)$$

Where $\boldsymbol{\Delta F}$ is the globally averaged OLR reduction for the snow surface emissivity case and $\boldsymbol{\sigma}$ is the Stefan-Boltzmann constant. With a global mean surface air temperature of $\boldsymbol{T = 209\,K}$, the estimated change in surface air temperature would be around 0.5 - 1 K.

Such a small temperature change is minor when compared to other uncertainties in simulating the Neoproterozoic Snowball climate. For example, the initiation of a Snowball Earth at a given CO_2 level is strongly sensitive to the orbital parameters or continental configuration used, both uncertain quantities for 700 – 600 Ma (Eberhard et al., 2023; Voigt et al., 2010). Additionally, the level of insolation or CO_2 concentration used in a model has a much larger effect on the simulated Snowball climate than surface spectral emissivity (Yang et al., 2012). Not accounted for in our calculations is the variability and uncertainty of CH_4 and N_2O concentrations in the Neoproterozoic, as these concentrations were set to 0 for simplicity in the original simulation. Possible rapid decreases in these greenhouse gases could instigate a decrease in radiative forcing of ~10 W m^{-2}, enough to trigger and maintain a Snowball climate

This article is protected by copyright. All rights reserved.

Author Manuscript

state (Roberson et al., 2011; Pierrehumbert et al., 2011). While the expected temperature change from including surface spectral emissivity for a snow-covered "hard" Snowball solution is essentially insignificant, the effect on Snowball formation scenarios with exposed ice surfaces could still be meaningful.

4.1 Applications to the Jormungand mechanism

Particularly, we speculate surface emissivity can strengthen simulations of the Jormungand mechanism proposed by Abbot et al. (2011). The Jormungand mechanism describes how a Snowball Earth stabilizes into a waterbelt state. Strong ice-albedo feedback cools the globe and pushes the ice line from the poles to the tropics. Eventually, the ice line reaches around 20^{o} latitude. At this latitude, the descending branch of the Hadley circulation cells causes precipitation to decrease. The lack of precipitation results in the ice boundary receiving significantly less snow than the ice surface of the rest of the globe. At this point in the Snowball Earth formation process, the surface is divided into three regions. From the poles to around 20^{o} north or south of the equator, the surface is snow-covered sea ice. Adjacent to the snow-covered ice regions, there is a region of bare sea ice not covered by snow due to the lack of precipitation in the descending branch of the Hadley cell, coined the BASIR (BAre Sea Ice Region) in Hörner & Voigt (2024). From the BASIR to the equator, there is open ocean. The albedo of the bare sea ice is lower than that of the snow-covered sea ice, so the ice-albedo feedback effect is decreased to an amount such that the climate is stabilized. The large shortwave albedo difference between snow and bare ice drives the Jormungand mechanism. Abbot et al. (2011) found that average broadband albedos for snow and ice of 0.79 and 0.45, respectively, can result in a stable Jormungand climate state.

The difference in OLR when snow and ice surface spectral emissivities are used presents an additional radiative effect that could strengthen the Jormungand mechanism. Based on the above calculation, changing the surface emissivity from snow to ice in the BASIR (from 5° N/S to 20° N/S) could reduce OLR by an average of 2.2 W m^{-2}. For the Jormungand state to be stable, the increased reflected shortwave radiation caused by surface albedo change due to ocean freezing must be offset to some extent. The reduction of OLR here can partly offset such an increase of outgoing shortwave radiation in the BASIR and, therefore, aid in counteracting the ice-albedo feedback. The difference in OLR between the snow surface and bare ice surface cases highlights the impact of precipitation in Snowball modeling. Figure 8 sketches the possible impact of surface spectral emissivity on the Jormungand mechanism using the estimates derived from our calculation for ice and snow surface types.

4.2 Applications to cold, dry climates

As shown by Chen et al. (2014) and Huang et al. (2018), polar regions of the present Earth are particularly impacted by changes in surface emission due to their low humidity (which leads to a small atmospheric opacity) and cold temperatures. The results shown here further support that surface emissivity can have a considerable impact on modeling cold and dry climates. As Snowball Earth is not the only era in the past with a cold and dry climate, we speculate that the representation of surface spectral emissivity could significantly affect other

This article is protected by copyright. All rights reserved.

Author Manuscript

paleoclimate modeling studies as well. For example, models of the last glacial maximum (LGM) have been used to constrain projections of climate change and climate sensitivity (e.g., Schmidt et al., 2014; Zhu et al., 2021). With more of the Earth's surface covered in glaciers, as in the LGM, the surface emissivity can matter, especially given the fact that ice has a surface emissivity of only around ~0.9 in the far-IR. Thus, surface spectral emissivity could play a role in the LGM simulations too. Additionally, the longwave radiation budget of the thin Martian atmosphere, another cold and dry climate, could be significantly affected by the representation of surface spectral emissivity, especially in the northern polar cap on Mars in warm seasons, which mainly consists of water ice mixed with dust. The simulated radiative balance of icy moons, such as Titan and Europa, could also be affected by the inclusion of surface spectral emissivity.

Acknowledgments

We thank the Editor and the three reviewers, including Dr. Daniel Koll and Dr. Charlie Zender, for their constructive and insightful comments, which have resulted in a clearer, more robust, and overall improved paper. We are indebted to Dr. Koll for suggesting the simple feedback estimation presented in Section 4. Additionally, we thank Dr. Aronne Merrelli for helpful discussion regarding far-IR transmissivities. The lead author DSZ would like to acknowledge the support of the Dean's Fellowship at the University of Michigan, College of Engineering. Coauthor XLH is supported in part by the U.S. Department of Energy, Office of Science, Office of Biological and Environmental Research, Climate and Environmental Science Division under Awards DE-SC0022117 to the University of Michigan.

Open Research

Data from a Snowball Earth simulation performed by JH and AV were used to represent Snowball conditions (Hörner and Voigt 2024). The ICON model was used for these simulations (Giorgetta et al., 2018). Surface emissivity data from Huang et al. (2016b) was used to represent ocean, ice, and snow surfaces. The MODTRAN radiative transfer model (Anderson et al., 2006; Berk et al., 1998; and Berk et al., 2005) was used to calculate the change in OLR when surface

This article is protected by copyright. All rights reserved.

Author Manuscript

spectral emissivity is included. Data from the NASA MERRA-2 reanalysis was used to illustrate typical humidity values in the modern Earth (Gelaro et al., 2017). Summaries of the results of the calculations performed, the data that is needed to create the figures, and a Jupyter notebook that demonstrates how to access the data and create the figures is stored in a repository hosted by the University of Michigan's Deep Blue data storage system at https://doi.org/10.7302/949x-tw78 (Zetterberg et al., 2025).

References

Abbot, D. S., Eisenman, I., & Pierrehumbert, R. T. (2010). The Importance of Ice Vertical Resolution for Snowball Climate and Deglaciation. *Journal of Climate*, *23*(22), 6100-6109. https://doi.org/10.1175/2010JCLI3693.1

Abbot, D. S., Voigt, A., & Koll, D. (2011). The Jormungand global climate state and implications for Neoproterozoic glaciations. *Journal of Geophysical Research*, *116*(D18103), https://doi.org/10.1029/2011JD015927

Abbot, D. S., Voigt, A., Li, D., Le Hir, G., Pierrehumbert, R. T., Branson, M., Pollard, D., & Koll, D. D. B. (2013). Robust elements of Snowball Earth atmospheric circulation and oases for life. *Journal of Geophysical Research: Atmospheres*, *118*(12), 6017-6027, https://doi.org/10.1002/jgrd.50540

Anderson, G., Berk, A., Harder, G., Fontenla, J., Shettle, E., Pilewski, P., et al. (2006). Atmospheric Sensitivity to Spectral Top-of-Atmosphere Solar Irradiance Perturbations, Using MODTRAN-5 Radiative Transfer Algorithm. Paper presented at American Geophysical Union, Fall Meeting, San Francisco, CA.

Berk, A., Bernstein, L. S., Anderson, G. P., Acharya, P. K., Robertson, D. C., Chetwynd, J. H., &

This article is protected by copyright. All rights reserved.

Author Manuscript

Adler-Golden, S. M. (1998). MODTRAN Cloud and Multiple Scattering Upgrades with Application to AVIRIS. *Remote Sensing of Environment*, *65*(3), 367-375. https://doi.org/10.1016/S0034-4257(98)00045-5

Berk, A., Gail, A. P. Acharya, P. K., Bernstein, L. S., Muratov, L., Lee, J., et al. (2005). MODTRAN 5: a reformulated atmospheric band model with auxiliary species and practical multiple scattering options: update. *Proceedings of the SPIE*, *5806*, 662-667. https://doi.org/10.1117/12.606026

Budyko, M. I. (1969). The effect of solar radiation variations on the climate of the Earth. *Tellus*, *21*(5), 611-619.

Chen, X., Huang, X., & Flanner, M. G. (2014). Sensitivity of modeled far-IR radiation budgets in polar continents to treatments of snow surface and ice cloud radiative properties. *Geophysical Research Letters*, *41*(18), 6530-6537. https://doi.org/10.1002/2014GL061216

Chen, Y. H., Huang, X., Chen, X., & Flanner, M. (2019). The Effects of Surface Longwave Spectral Emissivity on Atmospheric Circulation and Convection over the Sahara and Sahel. *Journal of Climate*, *32*(15), 4873-4890. https://doi.org/10.1175/JCLI-D-18-0615.1

Eberhard, J., Bevan, O. E., Feulner, G., Petri, S., van Hunen, J., & Baldini, J. U. L. (2023). Sensitivity of Neoproterozoic snowball-Earth inceptions to continental configuration, orbital geometry, and volcanism. *Climate of the Past*, *19*, 2203-2235. https://doi.org/10.5194/cp-19-2203-2023

Elsasser, W. M. (1942). *Heat Transfer by Infrared Radiation in the Atmosphere*, in *Harvard Meteorological Studies*, *6*, Harvard University Press: Harvard, Massachusetts.

This article is protected by copyright. All rights reserved.

Feldman, D. R., Collins, W. D., Pincus, R., Huang, X., & Chen, X. (2014). Far-infrared surface emissivity and climate. *Proceedings of the National Academy of Sciences*, *111*(46), 16,297-16,302. https://doi.org/10.1073/pnas.1413640111

Gelaro, R., McCarty, W., Suárez, M. J., Todling, R., Molod, A., Takacs, L., et al. (2017) The Modern-Era Retrospective Analysis for Research and Applications, Version 2 (MERRA-2). *Journal of Climate*, *30*(14), 5419-5454. https://doi.org/10.1175/JCLI-D-16-0758.1

Giorgetta, M. A., Brokopf, R., Crueger, T., Esch, M., Fiedler, S., Helmert, J., et al. (2018). ICON-A, the atmosphere component of the ICON Earth system model: I. Model description. *Journal of Advances in Modeling Earth Systems*, *10*(7), 1613–1637. https://doi.org/10.1029/2017MS001242

Hoffman, P. A., Abbot, D. S., Ashkenzy, Y., Benn, D. I., Brocks, J. J., Cohen, P. A., et al. (2017). Snowball Earth climate dynamics and Cryogenian geology-geobiology. *Science Advances*, *3*(11). https://doi.org/10.1126/sciadv.1600983

Hoffman, P. F., Kaufman, A. J., Halverson, G. P., & Schrag, D. P, (1998). A Neoproterozoic Snowball Earth. *Science 281*(5381), 1342-1346. https://doi.org/10.1126/science.281.5381.1342

Hoffman, P. F. & Schrag, D. P. (2002). The snowball Earth hypothesis: testing the limits of global change. *Terra Nova* (*14*), 129-155. https://doi.org/10.1046/j.1365-3121.2002.00408.x

Hörner, J., Voigt, A., & Braun, C. (2022). Snowball Earth initiation and the thermodynamics of sea ice. *Journal of Advances in Modeling Earth Systems*, *14*(8), e2021MS002734. https://doi.org/10.1029/2021MS002734

Hörner, J. & Voigt, A. (2024). Sea-ice thermodynamics can determine waterbelt scenarios for

This article is protected by copyright. All rights reserved.

Author Manuscript

Snowball Earth, *Earth System Dynamics*, *15*(2), 215-223. https://doi.org/10.5194/esd-15-215-2024

Huang, X., Chen, X., Zhou, D. K., & Liu, X. (2016a). An observationally based global band-by-band surface emissivity dataset for climate and weather simulations. *Journal of the Atmospheric Sciences*, *73*(9), 3541-3555. https://doi.org/10.1175/JAS-D-15-0355.1

Huang, X., Chen, X., Zhou, D., & Liu, X. (2016b). A global data set of surface spectral emissivity for GCM and NWP use [Dataset]. https://huang.engin.umich.edu/182-2/

Huang, X., Chen, X., Flanner, M., Yang, P., Feldman, D., & Kuo, C. (2018). Improved representation of surface spectral emissivity in a global climate model and its impact on simulate climate. *Journal of Climate*, *31*(9), 3711-3727. https://doi.org/10.1175/JCLI-D-17-0125.1

Iacano, M. J., Delamere, J. S., Mlawer, E. J., Shephard, M. W., Clough, S. A., & Collins, W. D. (2008). Radiative forcing by long-lived greenhouse gases: Calculations with the AER radiative transfer models. *Journal of Geophysical Research: Atmospheres*, *113*, D13103. https://doi.org/10.1029/2008JD009944

Kirshvink, J. L. (1992). Late Proterozoic low-latitude global glaciation: the snowball Earth. In *The Proterozoic Biosphere: A Multidisciplinary Study* (eds J. W. Schopf, C. Klein). Cambridge University Press, Cambridge, pp. 51-52.

Liu, Y. & Peltier, W. R. (2010). A carbon cycle coupled climate model of Neoproterozoic glaciation: Influence of continental configuration on the formation of a “soft snowball.” *Journal of Geophysical Research: Atmospheres*, *115*, D17111, https://doi.org/10.1029/2009JD013082

Liu, Y., Yang, J., Bao, H., Shen, B., & Hu, Y. (2020). Large equatorial seasonal cycle during

This article is protected by copyright. All rights reserved.

Author Manuscript

Marinoan snowball Earth. *Science Advances*, *6*(23), eaay2471.

Manzo, L., Zender, C., Tolento, J., & Whicker-Clarke, C. A. (2025). Improved representations of longwave surface emissivity to reduce surface and atmospheric heating biases in Earth system models. *Journal of Geophysical Research: Atmospheres*, *130*, e2024JD041776. https://doi.org/10.1029/2024JD041776

Mlawer, E. J., Taubman, S. J., Brown, P. D., Iacono, M. J., & Clough, S. A. (1997). Radiative transfer for inhomogeneous atmospheres: RRTM, a validated correlated-k model for the longwave. *Journal of Geophysical Research: Atmospheres*, *102*(D14), 16663-16682. https://doi.org/10.1029/97JD00237

Pierrehumbert, R. T. (2004). Climate dynamics of a hard snowball Earth. *Journal of Geophysical Research: Atmospheres*, *110*, D01111. https://doi.org/10.1029/2004JD005162

Pierrehuber, R. T., Abbot, D. S., Voigt, A., & Koll, D. (2011). Climate of the Neoproterozoic. Annual Review of Earth and Planetary Sciences, 39, 417-460. https://doi.org/10.1146/annurev-earth-040809-152447

Pincus, R., Mlawer, E. J., Delamere, J. S. Balancing Accuracy, Efficiency, and Flexibility in Radiation Calculations for Dynamical Models. (2019). *Journal of Advances in Modeling Earth Systems*, *11*, 3075-3089. https://doi.org/10.1029/2019MS001621

Roberson, A. L., Roadt, J, Halevy, I., & Kasting, J. F. (2011). Greenhouse warming by nitrous oxide and methane in the Proterozoic Eon. Geobiology, 9(4), 313-320. https://doi.org/10.1111/j.1472-4669.2011.00286.x

Schmidt, G. A., Annan, J. D., Bartlein, P. J., Cook, B. I., Guilyardi, E., Hargreaves, J. C., et al. (2014). Using palaeo-climate comparisons to constrain future projections in CMIP5.

This article is protected by copyright. All rights reserved.

Author Manuscript

Climate of the Past, *10*(1), 221-250, https://doi.org/10.5194/cp-10-221-2014

Schwarzschild, K., (1914). Diffusion and absorption in the sun's atmosphere. *Sitzungberichte der Koeniglichen Presussichen Akademie der Wissenschaften*, 1183-1200.

Sellers, W. D. (1969). A global climate model based on the energy balance of the Earth-atmosphere system. *Journal of Applied Meteorology*, *8*, 392-400.

Stevens, B. & Schwartz, S. E. (2012). Observing and Modeling Earth's Energy Flows. *Surveys in Geophysics*, *33*, 779-816. https://doi.org/10.1007/s10712-012-9184-0

Voigt, A., Abbot, D. S., Perrehumbert, R. T., & Marotzke, J. (2011). Initiation of a Marinoan Snowball Earth in a state-of-the-art atmosphere-ocean general circulation model. *Climate of the Past*, *7*, 249-263. https://doi.org/10.5194/cp-7-249-2011

Voigt, A. & Abbot, D. S. (2012). Sea-ice dynamics strongly promote Snowball Earth initiation and destabilize tropical sea-ice margins. *Climate of the Past*, *8*(6), 2079-2092. https:/doi.org/10.5194/cp-8-2079-2012

Yang, J., Peltier, W. R., & Hu, Y. (2012). The Initiation of Modern "Soft Snowball" and "Hard Snowball" Climates in CCSM3. Part I: The Influences of Solar Luminosity, CO_2 Concentration, and the Sea Ice/Snow Albedo Parameterization. Journal of Climate, 25(8), 2711-2736. https://doi.org/10.1175/JCLI-D-11-00189.1

Zetterberg, D. S., Huang, X., Hörner, J., & Voigt, A. (2025). Instantaneous radiative effect of surface long wave spectral emissivity in a Snowball Earth simulation [Data set], University of Michigan - Deep Blue Data. https://doi.org/10.7302/949x-tw78

Zhu, J., Otto-Bliesner, B. L., Brady, E. C., Poulsen, C. J., Tierney, J. E., Lofverstrom, M., &

This article is protected by copyright. All rights reserved.

Author Manuscript

DiNezio, P. (2021). Assessment of equilibrium climate sensitivity of the Community Earth System Model version 2 through simulation of the Last Glacial Maximum. *Geophysical Research Letters*, *48*, e2020GL091220. https://doi.org/10.1029/2020GL091220

Table 1.

	TCWV Snowball (mm)	TCWV Current (mm)	Current / Snowball (ratio)
Tropics	0.081	36.8	440
Mid-Lat	0.016	16.3	1040
Polar	0.0067	6.11	920

Table 2.

Band Number	Wavenumber Limits (cm^{-1})	Significant Absorbers
1	10-350	H_2O, O_3
2	350-500	H_2O
3	500-630	CO_2, H_2O
4	630-700	CO_2, H_2O, O_3
5	700-820	CO_2, O_3
6	820-980	CO_2
7	980-1,080	O_3, CO_2
8	1,080-1,180	O_3
9	1,180-1,390	H_2O, CO_2
10	1,390-1,480	H_2O
11	1,480-1,800	H_2O, O_3
12	1,800-2,080	CO_2, H_2O, O_3

Figure 1. Surface spectral emissivities of three surface types from Huang et al. (2016a). Snow here denotes the result of coarse snow in Huang et al. (2016a). (a) Spectral emissivity. (b) The

This article is protected by copyright. All rights reserved.

surface spectral emissivity averaged onto the first 12 bands used in the RRTMG LW, a radiation scheme widely adopted by climate models (Iacano et al., 2008).

Figure 2. (a) Climatological zonal-mean surface temperature of the simulation. (b) Climatological zonal-mean atmospheric temperature of the simulation. The simulated Snowball Earth climate is much cooler than the modern climate at every latitude and pressure level. As a result, a greater portion of the OLR will be emitted from the far-IR portion of the longwave spectrum, where surface emissivity is lower than in the mid-IR.

Figure 3. (a) Climatological zonal-mean TCWV of the simulation. (b) Climatological temperature profiles averaged for the tropical (30 S – 30 N), mid-latitude (30 – 60 S and 30 – 60 N), and polar (60 – 90 S and 60 – 90 N) regions. Symbol *x*'s denote the surface temperature for each region.

Figure 4. (a) Sensitivity of OLR to graybody surface emissivity vs total column water vapor for each region. y-axis units are change in TOA flux (W m^{-2}) over percent change in emissivity. (b) Relative sensitivity, with y-axis units being percent change in TOA flux over percent change in emissivity. For TCWV values less than 1 mm, as in the Snowball Earth, the magnitude of both the relative and absolute sensitivities to changes in surface emissivity are increased.

Figure 5. (a) Zonal-mean OLR difference in W m^{-2} when the blackbody surface is replaced by ice (orange) and snow (gray) surfaces, respectively. The blue dashed line represents the expected OLR difference at a given latitude if an open ocean surface appeared in the hard Snowball environment. Temperature and humidity profiles are taken from ICON aqua-planet simulation. (b) Same as (a) except for the relative difference of zonal-mean OLR (i.e. divided by the OLR of the blackbody case).

Figure 6. Percent change in OLR over RRTMG LW bands from the blackbody surface case when surface spectral emissivity is included in offline radiative transfer calculations for ice (a) and snow (b) surface types, respectively. The temperature and humidity profiles are taken from ICON aqua-planet simulation. The globally averaged OLR over each RRTMG LW band from the blackbody surface case is noted at the top of each panel in W m^{-2}. (c) A TOA mid-latitude emission spectrum from the MODTRAN calculations for the Snowball Earth environment with a blackbody surface. Each RRTMG band is marked by a different color to show its bandwidth.

Figure 7. Seasonal variations of zonal-mean differences in OLR when surface spectral emissivity is used versus the blackbody case. The results for January and July are shown in dashed and dotted lines, respectively, while the annual mean results are in solid lines. Results for the ice (orange) and snow (gray) surface types are shown together. The shadings denote the extent of the monthly variation (minimum to maximum) across all 12 calendar months. Note that all results are symmetric with respect to the equator, so for each case, only one hemisphere is shaded to improve the readability.

Figure 8. Adapted from Abbot et al. (2011) Figure 8. Diagrams of the Jormungand mechanism and resulting climate state. Gray represents snow, orange represents ice, and blue represents ocean. (a) The extra-tropics and the ascending branch of the Hadley cells near the equator

This article is protected by copyright. All rights reserved.

Author Manuscript

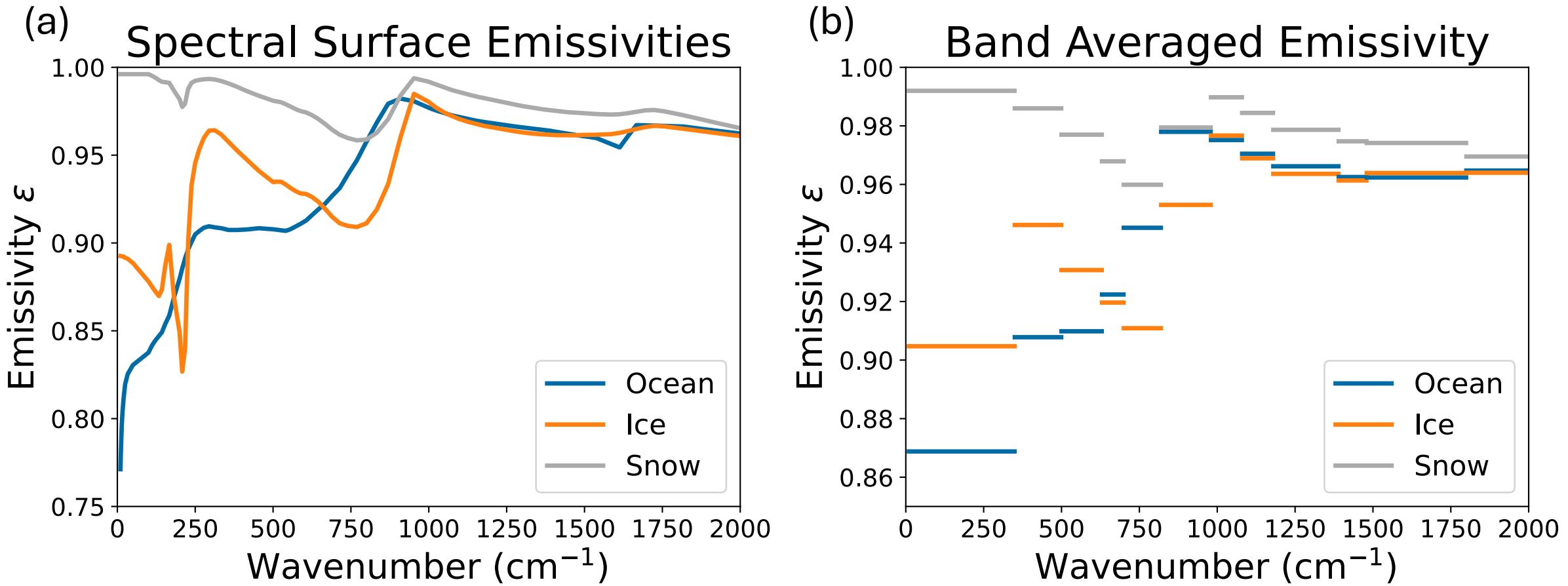
experience net precipitation (blue arrows). The BASIR (roughly 5° N/S to 20° N/S) at the descending branch of the Hadley cell experiences net evaporation (orange arrow), resulting in a lack of snow. (b) The decrease in OLR compared to the blackbody surface case when surface emissivities for snow in the extra-tropics and ice in the BASIR are used in offline radiative transfer calculations are labeled with the red arrows. Such a strong decrease in OLR in the BASIR could act to strengthen the Jormungand mechanism and stabilize a waterbelt climate state.

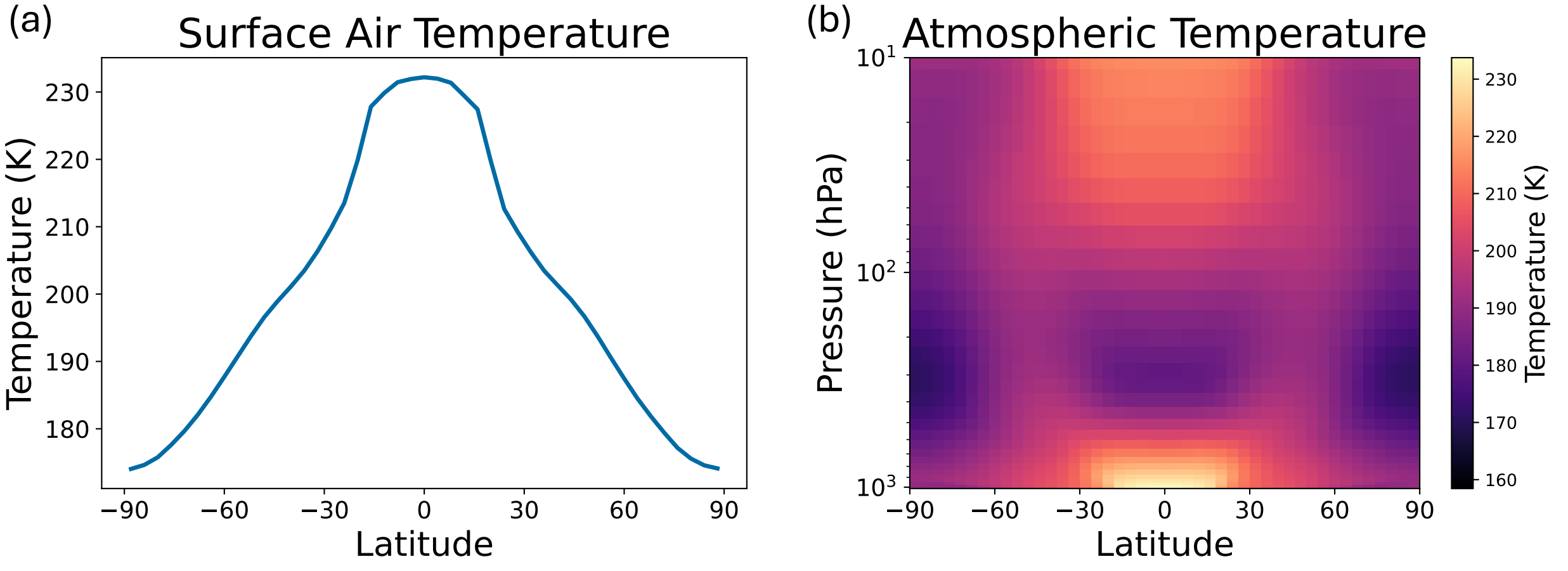
Table 1. Comparison of climatological Snowball Earth TCWV to current climatological TCWV, derived from NASA MERRA-2 reanalysis for 2006-2015.

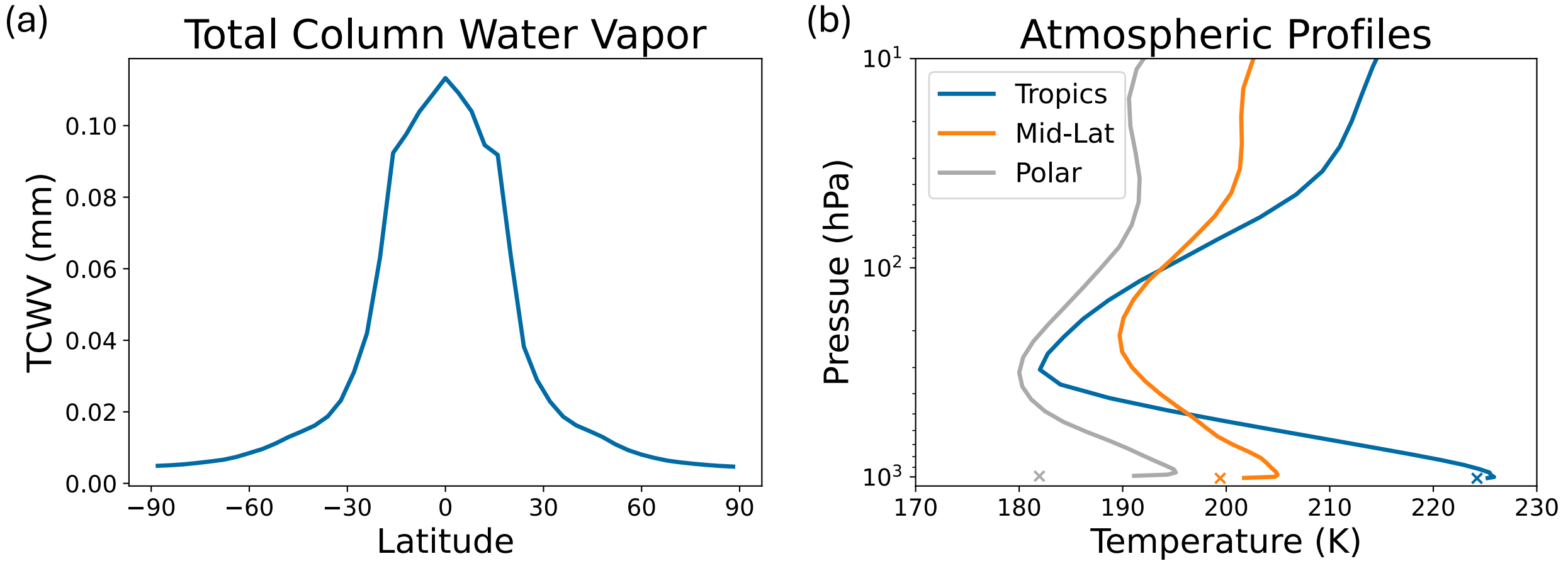
Table 2: Description of RRTMG bands, including wavenumber limits and significant absorbers. Adapted from Mlawer et al. (1997) Table 1.

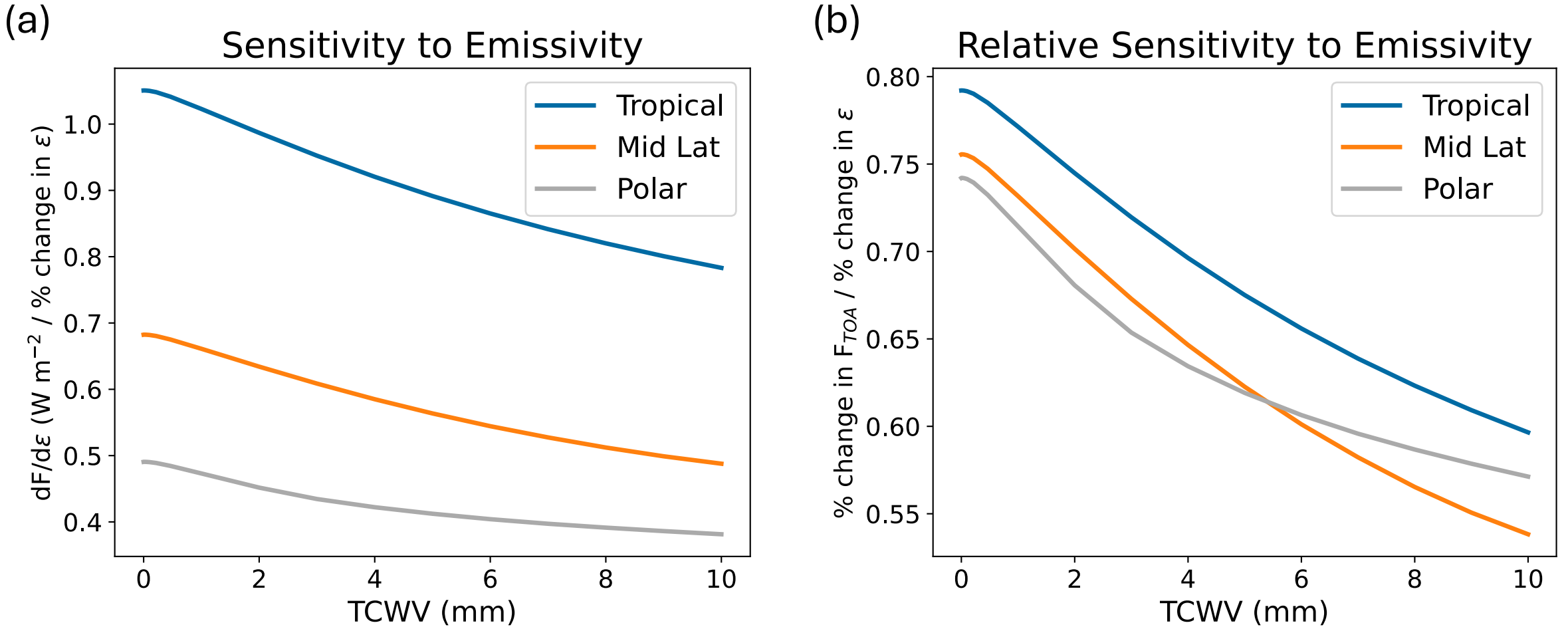
Author Manuscript

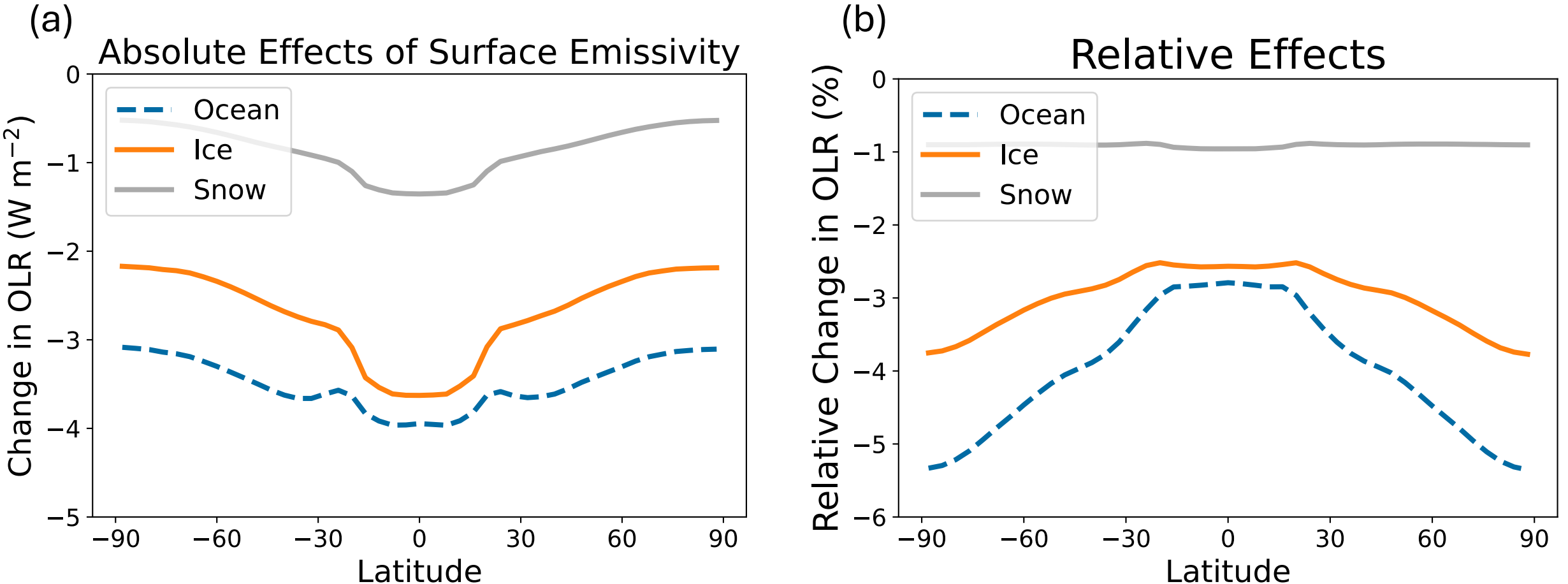
This article is protected by copyright. All rights reserved.

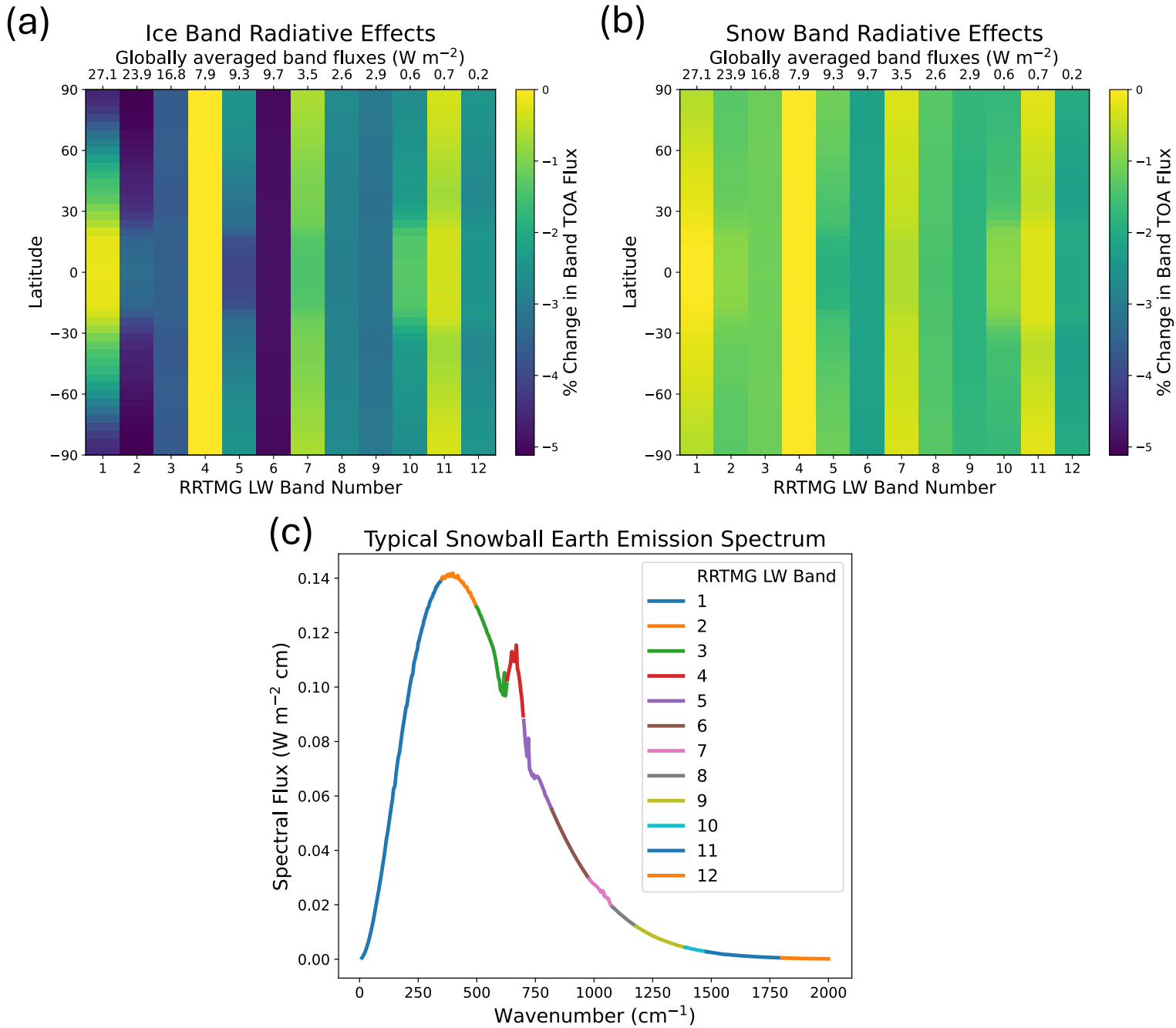

(a)
Spectral Surface Emissivities
Emissivity ε
1.00
0.95
0.90
0.85
0.80
0.75
0
250
500
750
1000
1250
1500
1750
2000
Wavenumber (cm^{-1})
Ocean
Ice
Snow
(b)
Band Averaged Emissivity
Emissivity ε
1.00
0.98
0.96
0.94
0.92
0.90
0.88
0.86
0
250
500
750
1000
1250
1500
1750
2000
Wavenumber (cm^{-1})
Ocean
Ice
Snow

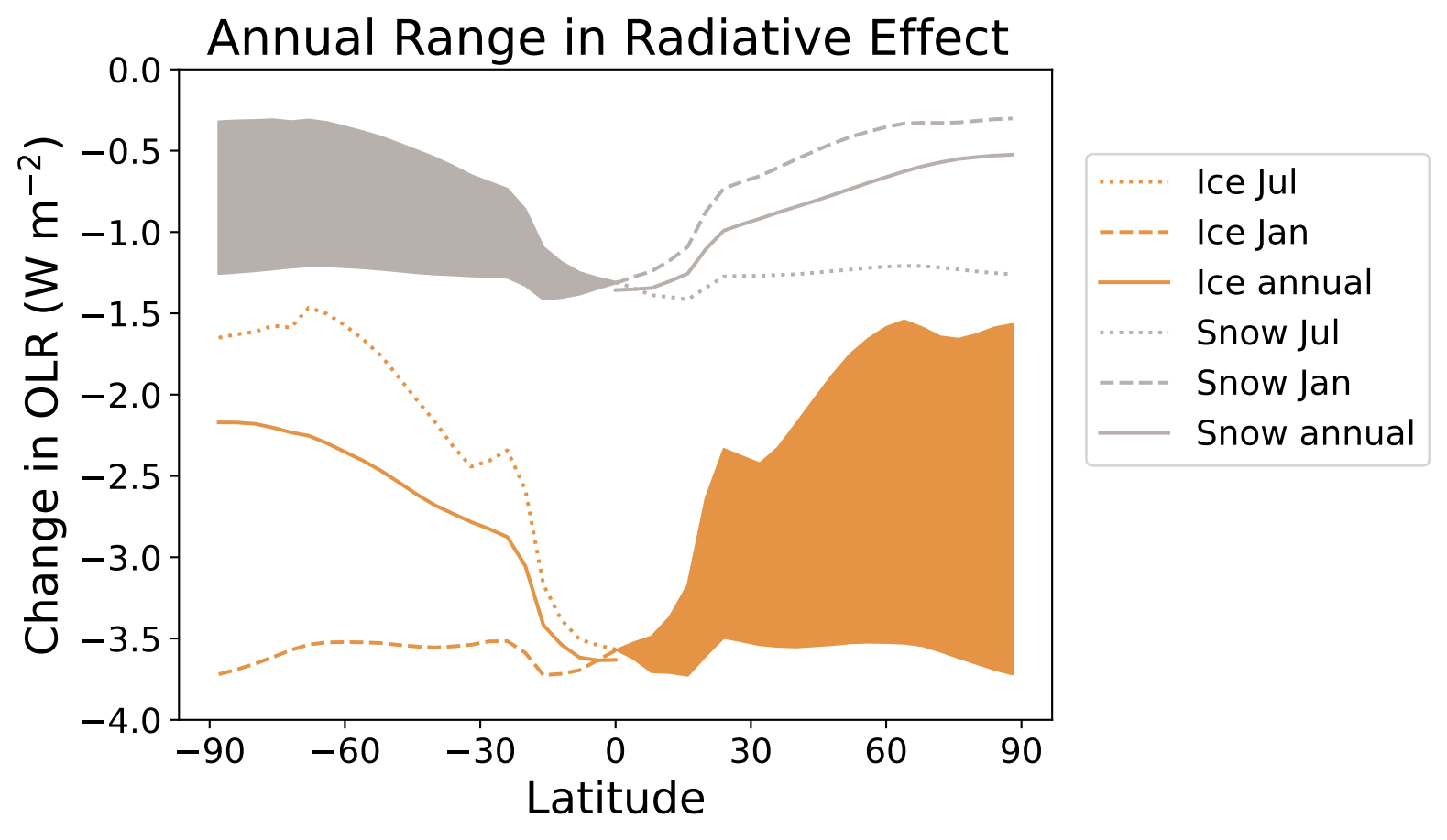

(a)
Surface Air Temperature
Temperature (K)
230
220
210
200
190
180
−90
−60
−30
0
30
60
90
Latitude
(b)
Atmospheric Temperature
Pressure (hPa)
10^1
10^2
10^3
−90
−60
−30
0
30
60
90
Latitude
Temperature (K)
230
220
210
200
190
180
170
160

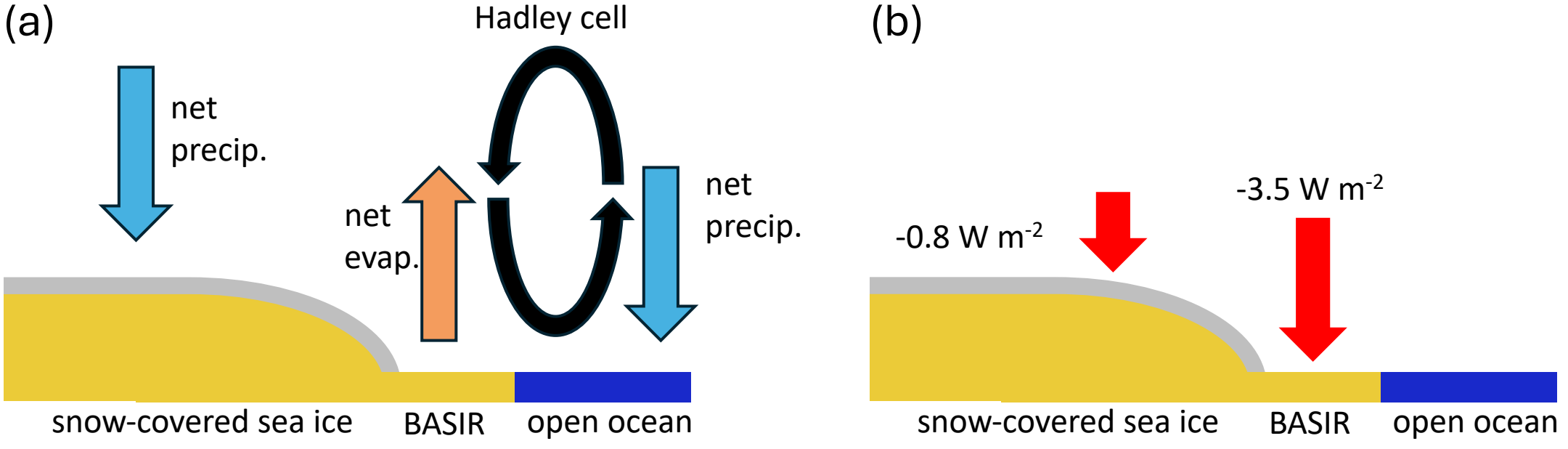

(a)
Total Column Water Vapor
TCWV (mm)
0.00
0.02
0.04
0.06
0.08
0.10
−90
−60
−30
0
30
60
90
Latitude
(b)
Atmospheric Profiles
Pressue (hPa)
10^1
10^2
10^3
Tropics
Mid-Lat
Polar
170
180
190
200
210
220
230
Temperature (K)


(a)
Sensitivity to Emissivity
dF/dε (W m^{-2} / % change in ε)
1.0
0.9
0.8
0.7
0.6
0.5
0.4
0
2
4
6
8
10
TCWV (mm)
Tropical
Mid Lat
Polar
(b)
Relative Sensitivity to Emissivity
% change in F_{TOA} / % change in ε
0.80
0.75
0.70
0.65
0.60
0.55
0
2
4
6
8
10
TCWV (mm)
Tropical
Mid Lat
Polar


(a)
Absolute Effects of Surface Emissivity
Change in OLR (W m^{-2})
Ocean
Ice
Snow
0
−1
−2
−3
−4
−5
−90
−60
−30
0
30
60
90
Latitude
(b)
Relative Effects
Relative Change in OLR (%)
Ocean
Ice
Snow
0
−1
−2
−3
−4
−5
−6
−90
−60
−30
0
30
60
90
Latitude


(a)
Ice Band Radiative Effects
Globally averaged band fluxes (W m^{-2})
27.1 23.9 16.8 7.9 9.3 9.7 3.5 2.6 2.9 0.6 0.7 0.2
Latitude
RRTMG LW Band Number
% Change in Band TOA Flux
(b)
Snow Band Radiative Effects
Globally averaged band fluxes (W m^{-2})
27.1 23.9 16.8 7.9 9.3 9.7 3.5 2.6 2.9 0.6 0.7 0.2
Latitude
RRTMG LW Band Number
% Change in Band TOA Flux
(c)
Typical Snowball Earth Emission Spectrum
RRTMG LW Band
Spectral Flux (W m^{-2} cm)
Wavenumber (cm^{-1})


Annual Range in Radiative Effect
Change in OLR (W m^{-2})
0.0
−0.5
−1.0
−1.5
−2.0
−2.5
−3.0
−3.5
−4.0
−90
−60
−30
0
30
60
90
Latitude
Ice Jul
Ice Jan
Ice annual
Snow Jul
Snow Jan
Snow annual


(a)
Hadley cell
net
precip.
net
evap.
net
precip.
snow-covered sea ice
BASIR
open ocean
(b)
-0.8 W m-2
-3.5 W m-2
snow-covered sea ice
BASIR
open ocean